Targeting and plasticity of mitochondrial proteins revealed by proximity-specific ribosome profiling

Christopher C. Williams *et al.*

Science **346**, 748 (2014);
DOI: 10.1126/science.1257522

LOCAL TRANSLATION

Targeting and plasticity of mitochondrial proteins revealed by proximity-specific ribosome profiling

Christopher C. Williams,* Calvin H. Jan,* Jonathan S. Weissman†

Nearly all mitochondrial proteins are nuclear-encoded and are targeted to their mitochondrial destination from the cytosol. Here, we used proximity-specific ribosome profiling to comprehensively measure translation at the mitochondrial surface in yeast. Most inner-membrane proteins were cotranslationally targeted to mitochondria, reminiscent of proteins entering the endoplasmic reticulum (ER). Comparison between mitochondrial and ER localization demonstrated that the vast majority of proteins were targeted to a specific organelle. A prominent exception was the fumarate reductase Osm1, known to reside in mitochondria. We identified a conserved ER isoform of Osm1, which contributes to the oxidative protein-folding capacity of the organelle. This dual localization was enabled by alternative translation initiation sites encoding distinct targeting signals. These findings highlight the exquisite in vivo specificity of organellar targeting mechanisms.

The vast majority of mitochondrial proteins (~99% in *Saccharomyces cerevisiae*) are encoded in the nuclear genome (*1*). These proteins are translated in the cytosol and must be sorted into the matrix, inner membrane (IM), intermembrane space (IMS), and outer membrane (OM) of the mitochondrion by a network of channels and chaperones. While the predominant view is that protein import into mitochondria occurs posttranslationally on unfolded polypeptides, cotranslational translocation has been demonstrated for some substrates (*2*). Moreover, ribosomes have been observed on the OM by electron microscopy (*3*), and numerous mRNAs associate closely with mitochondria (*4*–*6*), consistent with a broader role for cotranslational protein insertion.

To directly evaluate which proteins are translated on the surface of mitochondria in an unperturbed context, we applied the proximity-specific ribosome profiling technique (*7*). This approach involves in vivo biotinylation of Avi-tagged ribosomes that are in contact with a spatially localized biotin ligase (BirA), followed by affinity purification of biotinylated ribosomes and readout of translational activity by deep sequencing of ribosome-protected fragments. To mark ribosomes selectively on the mitochondrial surface, we fused BirA to the C terminus of *OM45*, a major component of the OM (Fig. 1A). Whereas a cytosolic BirA efficiently labeled both Avi-tagged large (Rpl16/uL13) and small (Rps2/uS5) subunits (*7*), Om45-BirA only biotinylated the large subunit, indicating that labeled ribosomes were constrained at the mitochondria with their peptide exit tunnels facing the OM (Fig. 1B). This pattern was observed for cotranslational import at the ER (*7*), arguing that ribosomes marked by Om45-BirA are engaged in protein translocation.

Proximity-specific profiling experiments were performedwith a brief (2-min) pulse of biotin in the absence of any translation inhibitors, to preserve the in vivo rates of translation and targeting. Of the enriched genes (fig. S1A), 87% were annotated as mitochondrial, and a clear subset of expressed mitop2 (*1*) mitochondrial reference genes (156 out of 551) were cotranslationally targeted (Fig. 1C and table S1). Each mitochondrial sublocalization was significantly enriched in cotranslationally targeted proteins ($P < 0.05$, Fisher's exact test). The IM proteins were distinct among sublocalizations (Fig. 1D); most IM proteins were cotranslationally targeted, whereas smaller subsets of OM, IMS, and matrix proteins were enriched (fig. S2A). By virtue of their transmembrane domains (TMDs), the IM proteins must simultaneously avoid aggregation in the cytosol and errant integration into other membranes. Cotranslational insertion may minimize the potential for toxicity associated with the accumulation of membrane proteins in the cytosol (*8*).

Omission of translation elongation inhibitors in the above experiments allowed us to define the proteins that were unambiguously translated at the mitochondrial surface. However, these were only a subset of the mRNAs that purify with mitochondria in the presence of the translation elongation inhibitor cycloheximide (CHX) (table S1) (*5*). We reasoned that by providing a prolonged time for ribosome–nascent chains (RNCs) to engage mitochondria, CHX pretreatment would yield a more comprehensive view of the mitochondrial proteome. Indeed, when we included CHX, we maintained mitochondrial specificity (fig. S1, B and C) but observed a large increase in the number of enriched proteins (Fig. 2A). For example, 68% (131 out of 191) of the mitop2-annotated matrix proteins were enriched compared to 27% (51 out of 187) without CHX (Figs. 2B and 1D).

We focused on the subset of genes that had a high probability of containing N-terminal mitochondrial matrix and IM protein-targeting sequences (MTSs), as predicted by MitoProt (*9*). The bimodal distribution of enrichments for this group raised the question of why some RNCs were translocation incompetent. We observed a clear difference in protein size between the enriched and depleted matrix proteins; the large majority of RNCs observed at the mitochondria were more than ~180 codons in length (Fig. 2C and fig. S3).

Mitochondrial proteins were selectively enriched across a wide range of expression levels (fig. S1C). This sensitivity allowed for the identification of 39 candidate mitochondrial proteins translated at the OM with no prior mitochondrial annotation in mitop2, Gene Ontology (GO), or Yeast GFP Fusion Localization databases (*1*, *10*, *11*) (Fig. 2A and table S1). These genes were more likely to contain MTSs, as predicted by Mitoprot (*9*), than nonenriched genes ($P = 0.002$, Mann-Whitney U test) (fig. S1D), supporting their candidacy as mitochondrial. Among this set was Hap1, a heme-responsive transcription factor (*12*). A Hap1-GFP (green fluorescence protein) fusion expressed from the endogenous locus was found both in the nucleus, as expected, and in the mitochondria, as predicted by our translational enrichments (Fig. 2D). Heme biosynthesis occurs in the mitochondria and is regulated by Hap1. Because MTS-mediated import requires an energized IM, Hap1 localization may allow for direct sensing of mitochondrial integrity. Hap1 sequestration in mitochondria could allow the cell to tune nuclear transcriptional activity through Hap1 localization (*13*).

We next investigated the evolution of mitochondrial protein localization among paralogs. *S. cerevisiae* underwent a whole-genome duplication (WGD) ~100 million years ago, making it well suited for exploring changes in protein localization between duplicate paralogs (termed ohnologs) (*14*). With the exception of the IM proteins, we found notable fluidity in the targeting of ohnologs to mitochondria that was not due to disparity in expression levels (Fig. 3A). By contrast, targeting of ohnologs to the ER rarely showed discrepancies between paralog pairs (Fig. 3B), emphasizing the relative plasticity of the mitochondrial proteome. In contrast to proteins residing in the ER or mitochondrial IM, matrix and cytosolic proteins have similar environments, which would allow proteins to function in either location.

We further exploited our mitochondrial and ER protein localization data sets to explore the extent to which individual proteins show dual localization between the two intracellular sites. The close physical association of these organelles makes the biochemical isolation of pure mitochondria

Department of Cellular and Molecular Pharmacology, Howard Hughes Medical Institute, California Institute for Quantitative Biosciences, Center for RNA Systems Biology, University of California, San Francisco, San Francisco, CA 94158, USA.
*These authors contributed equally to this work.
†Corresponding author. E-mail: jonathan.weissman@ucsf.edu

and microsomes challenging, confounding searches for dual localization in such preparations. For example, the ERMES complex, which tethers the ER and mitochondria (*15*), was originally thought to be exclusively mitochondrial. Proximity-specific ribosome profiling of the mitochondria and ER resolved components of the ERMES complex to their respective compartments and provided highly specific catalogs of

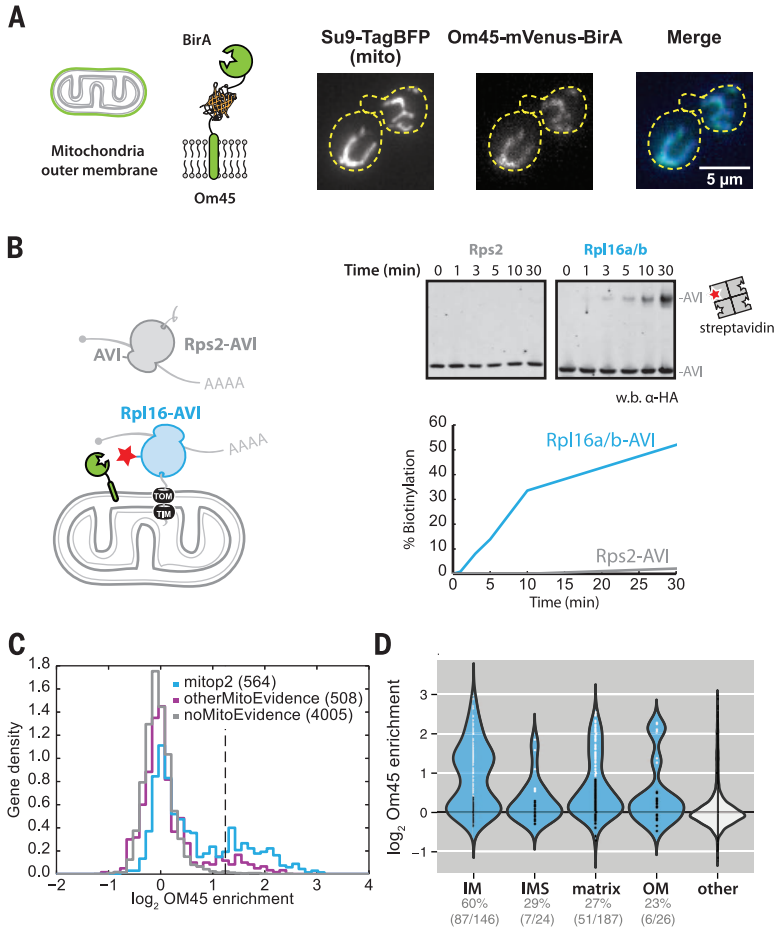

Fig. 1. Cotranslational mitochondrial protein targeting as revealed by proximity-specific ribosome profiling. (**A**) Localization of biotin ligase to the outer membrane. Schematic of the Om45 fusion protein and confocal fluorescence images of Om45-mVenus-BirA and Su9-TagBFP are shown. (**B**) Assessment of ribosome orientation at the mitochondrial outer membrane. The kinetics of Avi-tagged Rps2 (gray) and Rpl16a/b (blue) biotinylation by Om45-mVenus-BirA were determined by Western blot analysis of streptavidin-shift gels. (**C**) Histogram of $\log_2$ ratios for biotinylated footprints/input footprints in the absence of CHX. Genes annotated in the mitop2 reference set are shown in blue and enrichment threshold is shown as a dashed vertical line. Genes with mitochondrial GO cellular component terms not in mitop2 are shown in magenta. (**D**) Violin plot showing $\log_2$ gene enrichments for proteins grouped by their annotated location within mitochondria in the absence of CHX arrest. Gene enrichments are overlaid as points, with white and black colors indicating enrichment or disenrichment, respectively, as determined by subcompartment-specific Gaussian mixture modeling (fig. S2A) and quantified below the plot.

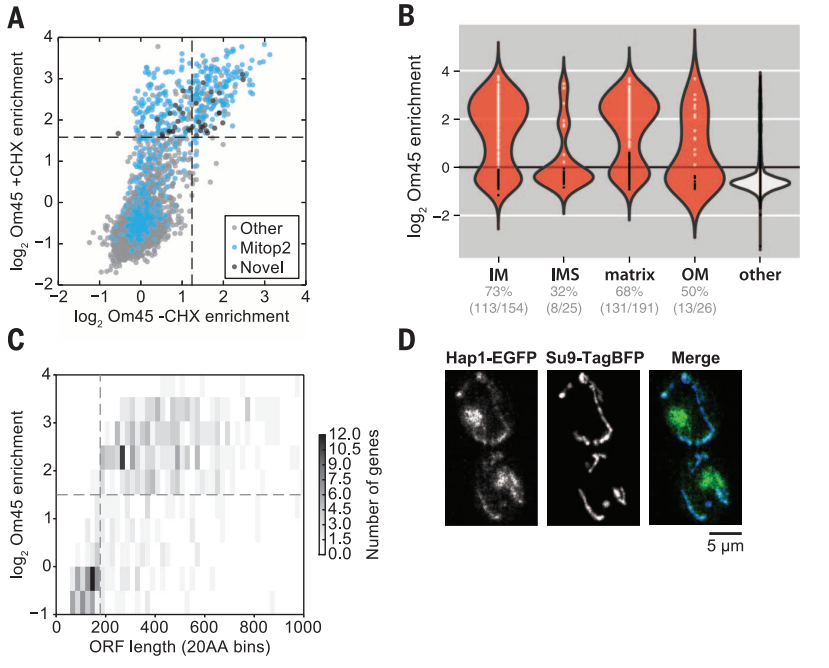

Fig. 2. Comprehensive characterization of RNC targeting to the mitochondria. (**A**) Scatter plot of $\log_2$ gene enrichments for footprints from ribosomes biotinylated by Om45-mVenus-BirA in the presence or absence of CHX. Novel genes represent those that were significantly enriched but had no known mitochondrial annotations. (**B**) Violin plot showing $\log_2$ gene enrichments for proteins grouped by their location within mitochondria in the presence of CHX arrest (as in Fig. 1D). Gene enrichments were determined by subcompartment-specific Gaussian mixture modeling (fig. S2B). (**C**) Two-dimensional histogram of genes binned by open reading frame length compared to their $\log_2$ gene enrichment in the presence of CHX. (**D**) Epifluorescence microscopy of Hap1-EGFP and Su9-TagBFP.

proteins at each organelle (Fig. 4, A and B, and fig. S4).

Very few proteins exhibited dual localization. Most proteins with both secretory and mitochondrial annotations (*10*) were cotranslationally inserted exclusively to the ER (Fig. 4B). Among the few counterexamples was the fumarate reductase *OSM1*. Although several studies suggest that Osm1 localizes exclusively to the mitochondria (*11*, *16*, *17*), high-throughput studies hint at a possible ER function. Specifically, a genetic-interaction data set indicated that *osm1*Δ shows a synthetic sick phenotype with a hypomorphic temperature-sensitive allele of *ERO1* (*18*) (fig. S5), the protein responsible for driving disulfide bond formation in the ER. Additionally, Osm1 is included in the N-glycoproteome, consistent with its entry into the secretory pathway (*19*). Our analysis of the glycosylation pattern of Osm1 and fluorescence microscopy of an endogenously expressed Osm1-GFP fusion protein demonstrated that Osm1 is localized to both the ER and mitochondria (Fig. 4, C and E).

Given the exquisite specificity of the vast majority of ER signal sequences (SSs) and MTSs, how is Osm1 efficiently targeted to both organelles? Ribosome profiling experiments using lactimidomycin (LTM), which leads to the accumulation of ribosomes at translation start sites (*20*), revealed that *OSM1* possesses two functional in-frame start codons predicted to encode either an ER (Met^{1}) or MTS (Met^{32}) signal (Fig. 4D). Mutation of the upstream methionine to alanine (Met1Ala) resulted in strict mitochondrial localization, whereas the Met32Ala mutant localized exclusively to the ER (Fig. 4E).

Osm1 homologs, including those of non-WGD yeast species, are predicted to contain SSs (*21*) (fig. S6), emphasizing the conserved ER localization of this class of fumarate reductases. Given the genetic interaction between *ERO1* and *OSM1*, an appealing function for this ER-localized form is to drive oxidative protein folding. Ero1 is a flavoprotein, and its reoxidation, following disulfide bond catalysis, can be driven by oxidized FAD (*22*, *23*). Furthermore, studies of oxidative folding under anaerobic conditions suggest that fumarate is the terminal electron acceptor and Osm1 generates free oxidized FAD via the reduction of fumarate (*24*). Consistent with this model, we found that the ER-form of Osm1 (Met32Ala), but not the mitochondrial-form (Met1Ala), supported growth under anaerobic conditions (Fig. 4F).

Proximity-specific ribosome profiling allowed us to elucidate several fundamental aspects of mitochondrial biogenesis. First, we discovered a major role for cotranslational targeting, but one that is most prominent for IM proteins. Second, we found that ohnologs encoding soluble proteins exhibit a high degree of fluidity in their mitochondrial localization, facilitating the exchange of function between the mitochondrial matrix and

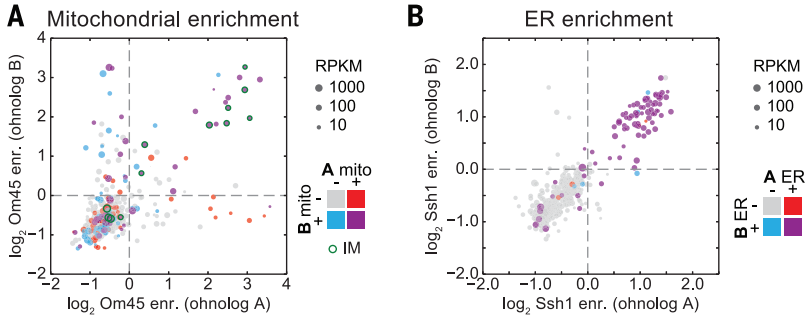

Fig. 3. Conservation of paralogous protein localization. (**A**) Scatter plot of mitochondrial $\log_2$ gene enrichments for ohnolog pairs, whose *x*- and *y*-axis assignment is arbitrary. Color codes indicate the expected ohnolog localizations based on existing evidence consolidated from mitop2, GO, and GFP annotations. Point size represents minimum expression level between paralogs. (**B**) As in (A), for ER enrichments.

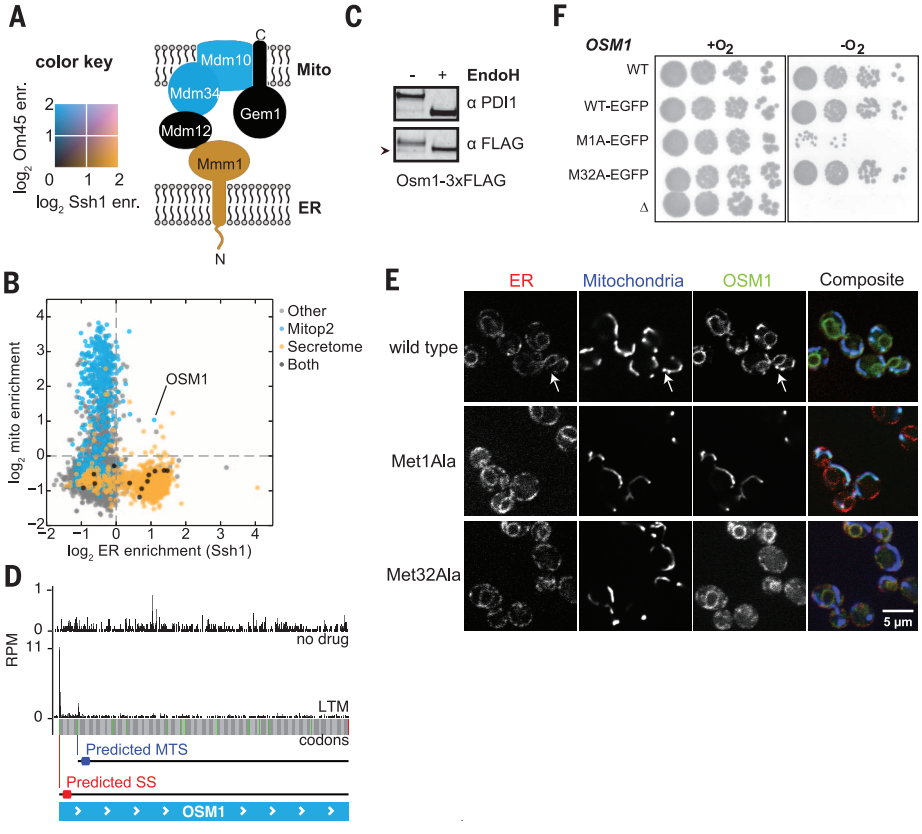

Fig. 4. Dual localization of proteins to the mitochondria and ER. (**A**) The color-mapped $\log_2$ enrichments for ribosome labeling by Om45 (blue) and Ssh1 (orange) are overlaid for members of the ERMES complex. (**B**) Scatter plot of ER enrichments compared to mitochondrial enrichments in the presence of CHX. Points are colored by their annotated localization. (**C**) Western blot analysis of N-linked glycans. Extracts from cells expressing Osm1-3xFLAG were blotted for PDI1 or FLAG with or without EndoH treatment. Arrowhead indicates an Osm1 band migrating below the size of the deglycosylated protein. (**D**) Ribosome occupancy of Osm1 with or without LTM treatment. In-frame AUG codons are shown in green; predicted localization of proteins made from the indicated start codon are shown. (**E**) Confocal fluorescence microscopy of Osm1-EGFP localization compared to ER (Sec63-mCherry) or mitochondria (Su9-BFP). Wild-type, Met1Ala, and Met32Ala variants of Osm1 are shown. (**F**) Analysis of signal requirements for Osm1 to support anaerobic growth as the sole fumarate reductase gene.

the cytosol. This plasticity may have facilitated or have been driven by the metabolic changes associated with a switch toward preferring fermentation over respiration that occurred after the WGD in budding yeast (the Crabtree effect) (*25*). Third, we demonstrated the exquisite specificity of protein targeting to the ER versus mitochondria in vivo. How targeting factors, such as SRP (*26*) and NAC (*27*), act on diverse RNCs to create this specificity in vivo remains an open question.

REFERENCES AND NOTES

1. M. Elstner, C. Andreoli, T. Klopstock, T. Meitinger, H. Prokisch, *Methods Enzymol.* **457**, 3–20 (2009).
2. T. D. Fox, *Genetics* **192**, 1203–1234 (2012).
3. R. E. Kellems, V. F. Allison, R. A. Butow, *J. Cell Biol.* **65**, 1–14 (1975).
4. M. Suissa, G. Schatz, *J. Biol. Chem.* **257**, 13048–13055 (1982).
5. P. Marc *et al.*, *EMBO Rep.* **3**, 159–164 (2002).
6. Y. Saint-Georges *et al.*, *PLOS ONE* **3**, e2293 (2008).
7. C. H. Jan, C. C. Williams, J. S. Weissman, *Science* **346**, 1257521 (2014).
8. O. Brandman *et al.*, *Cell* **151**, 1042–1054 (2012).
9. M. G. Claros, P. Vincens, *Eur. J. Biochem.* **241**, 779–786 (1996).
10. J. M. Cherry *et al.*, *Nucleic Acids Res.* **40**, D700–D705 (2012).
11. W.-K. Huh *et al.*, *Nature* **425**, 686–691 (2003).
12. L. Guarente, B. Lalonde, P. Gifford, E. Alani, *Cell* **36**, 503–511 (1984).
13. A. M. Nargund, M. W. Pellegrino, C. J. Fiorese, B. M. Baker, C. M. Haynes, *Science* **337**, 587–590 (2012).
14. K. Wolfe, *Nat. Genet.* **25**, 3–4 (2000).
15. B. Kornmann *et al.*, *Science* **325**, 477–481 (2009).
16. H. Muratsubaki, K. Enomoto, *Arch. Biochem. Biophys.* **352**, 175–181 (1998).
17. K. Enomoto, Y. Arikawa, H. Muratsubaki, *FEMS Microbiol. Lett.* **215**, 103–108 (2002).
18. M. Costanzo *et al.*, *Science* **327**, 425–431 (2010).
19. D. F. Zielinska, F. Gnad, K. Schropp, J. R. Wiśniewski, M. Mann, *Mol. Cell* **46**, 542–548 (2012).
20. N. Stern-Ginossar *et al.*, *Science* **338**, 1088–1093 (2012).
21. K. P. Byrne, K. H. Wolfe, *Genome Res.* **15**, 1456–1461 (2005).
22. E. Gross *et al.*, *Proc. Natl. Acad. Sci. U.S.A.* **103**, 299–304 (2006).
23. B. P. Tu, J. S. Weissman, *Mol. Cell* **10**, 983–994 (2002).
24. Z. Liu, T. Österlund, J. Hou, D. Petranovic, J. Nielsen, *Appl. Environ. Microbiol.* **79**, 2962–2967 (2013).
25. J. M. Thomson *et al.*, *Nat. Genet.* **37**, 630–635 (2005).
26. D. Akopian, K. Shen, X. Zhang, S. O. Shan, *Annu. Rev. Biochem.* **82**, 693–721 (2013).
27. M. del Alamo *et al.*, *PLOS Biol.* **9**, e1001100 (2011).

ACKNOWLEDGEMENTS

We thank members of the Weissman and P. Walter labs for discussion and E. Costa and V. Okreglak for critical reading of the manuscript. The University of California, San Francisco, Center for Advanced Technology and Nikon Imaging Center provided technical support. We thank C. Policarpi for assistance in strain construction and pilot ribosome profiling experiments, G. Brar for sharing unpublished ribosome profiling data, P. Walter for use of the Su9-TagBFP plasmid, and J. Horst for assistance with anaerobic growth conditions and equipment. This research was supported by the Center for RNA Systems Biology and the Howard Hughes Medical Institute. C.C.W. is an NSF Graduate Research Fellow. C.H.J. is the Rebecca Ridley Kry Fellow of the Damon Runyon Cancer Research Foundation (DRG-2085-11). Data are deposited in Gene Expression Omnibus under accession nos. GSE61011 and GSE61012.

SUPPLEMENTARY MATERIALS

www.sciencemag.org/content/346/6210/748/suppl/DC1
Materials and Methods
Figs. S1 to S6
Tables S1 to S5
References (*28*–*31*)

16 June 2014; accepted 12 September 2014
10.1126/science.1257522

QUALITY CONTROL

Quality control of inner nuclear membrane proteins by the Asi complex

Ombretta Foresti,[1,2] Victoria Rodriguez-Vaello,[1,2] Charlotta Funaya,[3] Pedro Carvalho[1,2]*

Misfolded proteins in the endoplasmic reticulum (ER) are eliminated by a quality control system called ER-associated protein degradation (ERAD). However, it is unknown how misfolded proteins in the inner nuclear membrane (INM), a specialized ER subdomain, are degraded. We used a quantitative proteomics approach to reveal an ERAD branch required for INM protein quality control in yeast. This branch involved the integral membrane proteins Asi1, Asi2, and Asi3, which assembled into an Asi complex. Besides INM misfolded proteins, the Asi complex promoted the degradation of functional regulators of sterol biosynthesis. Asi-mediated ERAD was required for ER homeostasis, which suggests that spatial segregation of protein quality control systems contributes to ER function.

Misfolded proteins in the membrane and lumen of the endoplasmic reticulum (ER) are eliminated by ER-associated protein degradation (ERAD) (*1*, *2*). In *Saccharomyces cerevisiae*, two ubiquitin ligase complexes, Hrd1 and Doa10, are involved in ERAD and show different specificity for misfolded proteins (*1*–*5*). Proteins with a misfolded domain in the cytosol (ERAD-C substrates) are targeted to degradation by the Doa10 complex, whereas proteins with misfolded domains in the membrane (ERAD-M) or lumen (ERAD-L) of the ER are ubiquitinated by the Hrd1 complex. The ubiquitin-conjugating (E2) enzyme Ubc7 is part of both complexes, and consequently *ubc7*Δ cells are defective in all ERAD branches. Besides misfolded proteins, ERAD is involved in the degradation of specific folded proteins, such as the sterol biosynthetic enzyme HMG-CoA reductase, in response to certain physiological stimuli (*2*).

To identify endogenous substrates of the different ERAD branches in *S. cerevisiae*, we compared the proteomes of *doa10*Δ, *hrd1*Δ, and *ubc7*Δ cells with the use of SILAC (stable isotope labeling by amino acids in culture) followed by quantitative proteomics (*6*) (table S1). This analysis revealed a set of proteins whose steady-state levels in *doa10*Δ or *hrd1*Δ were comparable to those in wild-type (*wt*) cells but were higher in *ubc7*Δ mutants relative to *wt* cells (table S2). Among these proteins were Erg11 (lanosterol 14-α-demethylase) and Nsg1, both involved in ergosterol synthesis (Fig. 1A and table S2). Given that Erg11 is an ER membrane protein and that sterol biosynthesis is regulated by ERAD (*2*), we tested whether Erg11 was an ERAD substrate. In *wt* cells, a plasmid-borne, functional Erg11 fused to hemagglutinin (Erg11-HA) was degraded with a half-life of ~60 min (Fig. 1B and fig. S1A). We observed similar kinetics of degradation in *doa10*Δ, *hrd1*Δ, or even *doa10*Δ *hrd1*Δ double mutant cells (Fig. 1B and fig. S1B). In agreement with the SILAC analysis, the degradation of Erg11-HA was delayed in *ubc7*Δ, indicating that this E2 works with an uncharacterized ubiquitin ligase (E3). The degradation of Erg11 was further reduced by simultaneous mutation of *UBC7* and *UBC4*, indicating that these E2s have redundant roles in Erg11 ERAD (fig. S3).

The ERAD of all known membrane-bound substrates requires the Cdc48 adenosine triphosphatase (ATPase). Inactivation of Cdc48 function in cells bearing the temperature-sensitive *cdc48-3* allele showed impaired degradation of Erg11-HA (Fig. 1C). These findings suggest the existence of an ERAD branch independent of the known E3s Hrd1 and Doa10 but requiring Ubc7 and Cdc48.

Besides the canonical ERAD E3s, there is a third ER integral membrane E3. This is composed of two paralog proteins, Asi1 and Asi3, localized to the inner nuclear membrane (INM) (*7*, *8*). The INM is connected to the rest of the ER membrane at nuclear pores, which restrict the exchange of proteins between the nucleus and cytoplasm and between the INM and the rest of the ER (*9*). Consequently, the INM defines a specialized ER subdomain enriched in proteins with nuclear functions. Indeed, *ASI1*, *ASI3*, and several *ASI* (amino acid signaling–independent) mutants were originally identified as defective in transcriptional repression of amino acid permeases (AAPs) (*10*). The effect of Asi1 and Asi3 on AAP expression appears to be achieved by controlling the binding of the transcription factors Stp1 and Stp2 to the promoter of AAP genes without affecting their localization or stability (*7*, *8*). This repression of AAPs requires Asi2, another INM protein (*8*).

Deletion of *ASI1*, *ASI2*, or *ASI3* (but not of other *ASI* genes) blocked the degradation of Erg11

[1]Cell and Developmental Biology Programme, Centre for Genomic Regulation (CRG), Carrer del doctor Aiguader 88, 08003 Barcelona, Spain. [2]Universitat Pompeu Fabra, Carrer del doctor Aiguader 88, 08003 Barcelona, Spain. [3]Electron Microscopy Core Facility, European Molecular Biology Laboratory, 69117 Heidelberg, Germany.
***Corresponding author. E-mail: pedro.carvalho@crg.eu**